J Nanopart Res (2015) 17:397
DOI 10.1007/s11051-015-3201-4

RESEARCH PAPER

In situ synthesis of Cu_2O and Cu nanoparticles during the thermal reduction of copper foil-supported graphene oxide

R. Ortega-Amaya · Y. Matsumoto · M. A. Pérez-Guzmán · M. Ortega-López

Received: 20 June 2015 / Accepted: 28 September 2015

Abstract This work describes a novel method to prepare reduced graphene oxide (rGO) sheets decorated with copper oxide and copper nanoparticles, by annealing copper foil-supported graphene oxide (GO) under an Ar atmosphere. The GO reduction level, the predominant Cu or Cu_2O compound, and the particle size strongly depend on the process temperature. Scanning electron microscopy and X-ray diffraction analysis revealed that rGO–Cu_2O and rGO–Cu nanocomposites developed on the Cu foil surface at the annealing temperatures of 200–600 and 800–1000 °C range, respectively. Raman spectroscopy corroborates the effective GO reduction.

Keywords Graphene oxide · Thermal reduction · Nanocomposite · Copper · Copper oxide · Nanoparticles

R. Ortega-Amaya (✉) · Y. Matsumoto · M. Ortega-López
SEES, Electrical Engineering Department, Centro de Investigación y de Estudios Avanzados del IPN, Av. IPN 2508, Col. San Pedro Zacatenco, 07360 Mexico City, Mexico
e-mail: ortegaa@cinvestav.mx

Y. Matsumoto · M. A. Pérez-Guzmán · M. Ortega-López
Nanoscience and Nanotechnology Program, Centro de Investigación y de Estudios Avanzados del IPN, Av. IPN 2508, Col. San Pedro Zacatenco, 07360 Mexico City, Mexico

Introduction

Graphene-based materials such as graphene oxide (GO) and graphene/inorganic nanoparticle composites are intensively studied due to their extraordinary physicochemical properties, which hold promise for applications in technological areas such as biomedical, energy, environmental remediation, and electronics (Allen et al. 2009; Bai and Shen 2012; Choi et al. 2012; Li et al. 2014; Neo and Ouyang 2013; Xu et al. 2013). Pristine graphene has mostly been studied for advanced electronics. For other applications than those, graphene needs to be functionalized because of its strongly hydrophobic character (Cai et al. 2012; Wu et al. 2013). Indeed, the recent interest in modifying the electronic properties of graphene has fueled research on graphene chemical doping by attaching specific functional groups at graphene plane (Liu et al. 2011).

Currently, GO is considered an important precursor for graphene mass production and chemically modified graphene, which includes the reduced version of GO (rGO; Casabianca et al. 2010; Pei and Cheng 2012).

GO is obtained by chemical exfoliation of graphite under strongly oxidative processes (Dreyer et al. 2010), so that the final product comprises GO nanosheets with a disrupted conjugation, containing hydroxyl and epoxide groups on the basal plane and carboxyl and carbonyl groups at the sheet edge (Compton and Nguyen 2010).

Techniques used to reduce GO include thermal annealing under an inert atmosphere (Zhao et al. 2012),

Published online: 05 October 2015

chemical treatment using strong (Park et al. 2011) or green reductive reagents (Fernández-Merino et al. 2010), and electrochemical reduction (Guo et al. 2009). In general, the above methods do not completely remove functional groups from GO, producing so-called partially reduced GO (rGO; Singh et al. 2011).

Nowadays, GO and rGO have emerged as promising materials to obtain a variety of nanocomposites together with inorganic and organic nanostructures (Menchaca-Campos et al. 2013; Shi et al. 2011; Stankovich et al. 2006).

In this work, we report our attempts to reduce GO using copper foils as substrate. Surprisingly, besides reducing effectively GO, copper and copper oxide nanostructures were developed during the annealing process. We believe that this is a useful and novel method to prepare rGO sheets decorated with Cu or Cu_2O nanoparticles. In the proposed method, the GO sheets are first prepared by graphite chemical exfoliation and then annealed under an Ar atmosphere using Cu foil-supported GO. Interestingly, well-crystalized Cu-based nanoparticles developed at temperatures as low as 200 °C, but their predominant phase strongly depended on the annealing temperature. In fact, Cu_2O and Cu were predominant ones at 200–600 and 800–1000 °C, respectively.

The physical properties of the obtained materials were assessed by using X-ray diffraction (XRD), Raman spectroscopy, and Fourier transform infrared spectroscopy (FT-IR).

Copper-based nanostructures grown on Cu foils were recently reported by Dong et al. (Dong et al. 2014). They prepared Cu_2O nanoparticles-decorated rGO nanocomposites using a Cu foil immersed in a GO aqueous dispersion, under hydrothermal conditions at 160–240 °C for 24 h. Hien et al. (Hien et al. 2013) synthesized copper or copper oxide nanowires using copper-supported etched-graphene by a hot-plate heating method under oxidative conditions, at temperatures around 450 °C.

Materials and methods

Materials

Graphite flakes (+100 mesh), sodium nitrate (≥99 %), potassium permanganate (≥99 %), and hexane (≥99 %) were purchased from Sigma-Aldrich. Sulfuric acid (95–98 %) was obtained from Reproquifin. Hydrogen peroxide (30 %), acetone (99.77 %), and copper foil (99.99 %) were obtained from J. T. Baker. Ethanol (99.5 %) was purchased from Reasol. All reagents were used as received without further purification.

Synthesis of GO

GO was synthesized by a modified Hummers method (Chen et al. 2010; Hummers and Offeman 1958). Briefly, graphite flakes (2 g), $NaNO_3$ (1 g), and concentrated H_2SO_4 (46 ml) were added in an Erlenmeyer flask, under stirring in an ice bath. Then $KMnO_4$ (6 g) was slowly added under stirring condition, and the temperature of the system was controlled at 20 °C. After 5 min, the mixture was removed from the ice bath and heated at 35 °C for 1 h. Next, 92 ml of water was slowly added into the system, and stirring was maintained for 15 min. Then, 140 ml of water was added at 60 °C, as well as 5 ml of 30 % solution of H_2O_2. Finally, the resulting mixture was centrifuged (4000 rpm for 30 min), and the supernatant was decanted away. The yellow–brown product was washed with warm water until pH 7 was reached. Finally, the product material in an aqueous medium was treated by mild ultrasound for 2 h.

Thermal reduction and decoration of GO

Prior to GO deposition, the Cu foil (0.02 mm thick and 1×1 cm^2) was cleaned by sequential sonication in hexane, acetone, and ethanol. The sample for GO reduction was prepared as follows. The initial GO dispersion was water evaporated using a rotary evaporator (BUCHI R-200) to get a 2 mg/ml concentrated dispersion and then drop-casted on the cleaned Cu foil to form a thin film. Before the high-temperature process, the sample was dried at 80 °C for 15 min under nitrogen flux.

The reduction process was carried out in an atmospheric pressure CVD apparatus equipped with a quartz tube. The annealing process was performed at 200, 400, 600, 800, and 1000 °C under an inert atmosphere of Ar for 1 h. In all cases, the GO film underwent a color change from brown to black after the thermal process. For characterization, the rGO films were peeled off with stainless steel tweezers and stored under environment conditions and then analyzed after one month.

Characterization

The structure and morphology were studied using XRD (X'Pert Pro with Cu Kα radiation), field emission scanning electron microscopy (FESEM, Zeiss Auriga), and energy dispersive X-ray spectrometry (EDS, Bruker Xflash 5010 detector) was used to characterize composition. Raman spectra were recorded with a Horiba Jobin–Yvon HR800 Raman apparatus, using a 50× objective lens with 532 nm laser excitation. FT-IR was done on KBr-supported sample pellets using a Perkin-Elmer spectrum 100.

Results and discussion

XRD characterization

The thermal annealing of the GO–Cu foil system produces a hybrid inorganic–organic nanocomposite consisting of rGO sheets decorated with Cu or Cu_2O nanoparticles; the inorganic dominant phase depended on the annealing temperature. This was corroborated by means of XRD measurements.

Figure 1 shows the XRD patterns of the as-deposited GO (a) and annealed samples at 200–1000 °C (b–f). The XRD pattern of the as-deposited GO displays the typical diffraction peak at $2\theta = 10.9°$, which has usually been attributed to the (002) reflection of samples comprising stacked GO sheets (Hadadian et al. 2014). After the annealing process, the peak shifts toward the 24–26° interval as the annealing temperature increases, hence the interlayer separation decreases with temperature. Previous studies on the thermal reduction of GO sheets prepared by oxidative exfoliation of graphite revealed that the GO interlayer separation was larger than that of graphite, due to intercalation of H_2O and functional groups (Bose et al. 2012; Notley 2012). Furthermore, the GO lattice as well as interlayer distance became as those of graphite [JCPDS 56–159] as the functional groups were thermally detached from graphene plane (Moon et al. 2010).

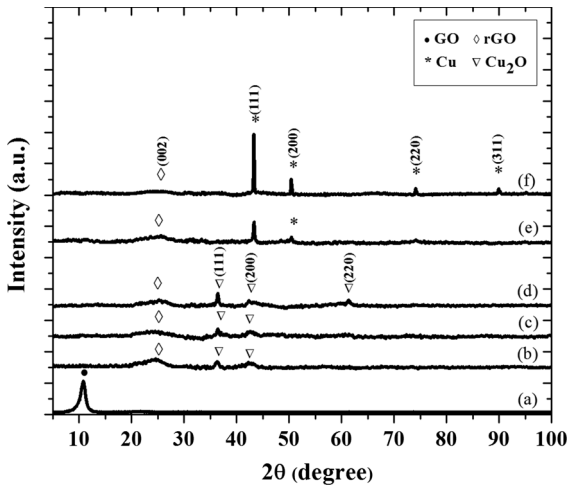

Fig. 1 XRD patterns of (*a*) the as-deposited GO and annealed samples at (*b*) 200, (*c*) 400, (*d*) 600, (*e*) 800, and (*f*) 1000 °C, for 1 h

Therefore, XRD testify the effective reduction of GO. In all cases, the interlayer distance of our samples was larger than that graphite (3.4 Å). An interlayer distance of 8.1 Å was calculated for GO by using the Bragg diffraction formula and the XRD data of Fig. 1a. For annealed samples, on the other hand, the estimated interlayer distances varied from 3.63 to 3.46 Å as the annealing temperature ranged from 200 to 1000 °C. The decrease in the interlayer separation appears to be correlated to the reduction process of GO, as suggested by the Raman spectra of samples (see Fig. 3 below), the smaller is the interlayer distance, the more reduced is the material. A similar behavior was previously reported (Huh 2011; Na et al. 2015; Some et al. 2013).

Notice that the (002) peak intensity decreases with the annealing temperature probably due to a change in the stacking of GO caused by the reduction and the composite formation, as reported by other workers (Hu et al. 2013; Mai et al. 2011; Xu et al. 2009).

In regarding to the Cu-related phases, XRD patterns in Fig. 1 show that Cu_2O dominates at lower temperatures (200, 400, and 600 °C), because all discernible peaks could be associated to the Cu_2O cubic phase [JCPDS 5–667]. The diffraction peaks at $2\theta = 36.4°$, 42.3°, and 61.3° corresponded to (111), (200), and (220) planes, respectively. The XRD patterns of the high-temperature samples (800 and 1000 °C) displayed diffraction peaks of the cubic Cu [JCPDS 4–836]. The peaks located at $2\theta = 43.3°$, 50.4°, 74.1°, and 89.9° could be ascribed to (111), (200), (220), and (311) planes, respectively. It was also observed that, the FWHM peak decreased with the annealing temperature, indicating the particle size increased with temperature.

Raman and FT-IR characterization

Figure 2 displays the typical FESEM images of (a) the bare Cu foil support and (b) as-deposited GO on the Cu foil after being annealed at 80 °C. The bare surface had a granular morphology with particles 7–18 nm in size. According to the EDS analysis, (not shown here) the Cu foil surface comprised carbonaceous species as ad-impurities and oxygen probably forming copper oxide.

The GO morphology consisted of crumpled and stacked sheets as indicated for Fig. 2b.

The effective reduction of GO was assessed by Raman spectroscopy. It is well known that Raman spectra of graphitic materials, including GO, exhibit the typical G and D bands which are associated with in-plane vibrations of carbon sp^2 bonds and structural defects, respectively. For GO, the reported wavenumber localization of G and D bands are around 1600 and 1350 cm^{-1}, respectively (Sobon et al. 2012). These bands change in position and intensity as oxygenated groups are detached to restore the graphene structure. Particularly, the G and D bands red shift, and the intensity ratio, I(D)/I(G), increases as reduction progresses (Zhenyuan et al. 2013).

The Raman spectra of the samples prepared in this work (Fig. 3) all exhibited the above mentioned features. The as-deposited GO displayed G and D bands at 1598 and 1357 cm^{-1} in good agreement with the wavenumber localization reported by Chen et al. (Chen et al. 2010), for G and D bands, respectively. It was also seen that G peak underwent a regular red shift from 1597 to 1587 cm^{-1} as the annealing temperature increased in the 200–1000 °C range. For the D band, a significant red shift was only observed at annealing temperatures higher than 400 °C. For samples annealed at 200 and 400 °C, the D band remain localized at the same wavenumber value as the as-deposited sample (1357 cm^{-1}), while it shifted 1342 cm^{-1} for annealing temperatures higher than 400 °C.

In summary, the above described behavior for the G and D bands corroborates that GO effectively reduces with temperature, and that the reduction level increases as annealing temperature does. The gradual red shift of the G band suggests the reduction of GO and the recovery of the sp^2 domain, in the case of the D band shift is associated with the size of the in-plane sp^2 domain (Chen and Yan 2010; Zhang et al. 2012). Likewise, the increase in the I(D)/I(G) ratio from 0.91 to 1.20 indicates the formation of numerous aromatic domains of smaller overall size in graphene (Stankovich et al. 2007).

It is noteworthy that the Cu_2O phase was not detected by means of Raman spectroscopy, because no characteristic signals of Cu_2O ($\sim$219, 400 and 624 cm^{-1}) (Deng et al. 2012) are discernible in the Raman spectra of our samples (Fig. 3). Similar results were obtained by Dong et al. (Dong et al. 2014) in well-coated rGO–Cu_2O nanoparticles. The presence of metallic Cu at 800–1000 °C suggests that it could exist not as a bare nanoparticle, but as a core-shelled rGO–Cu nanostructure, the rGO-coating protecting to Cu from oxidation.

The FT-IR technique allows for identifying the functional groups bound to the GO sheets. Figure 4 shows the IR spectra of (4a) the as-deposited GO and (4b–f) annealed GO at different temperatures. The IR spectrum of the as-deposited GO (Fig. 4a) exhibits the O–H stretching vibrations (3300 cm^{-1}), C=O

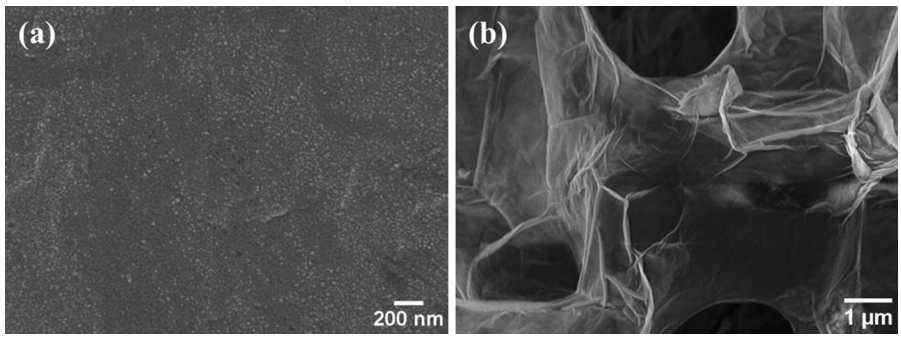

Fig. 2 FESEM images of (**a**) the surface Cu foil after being cleaned (**b**) as-deposited GO on Cu foil after drying at 80 °C

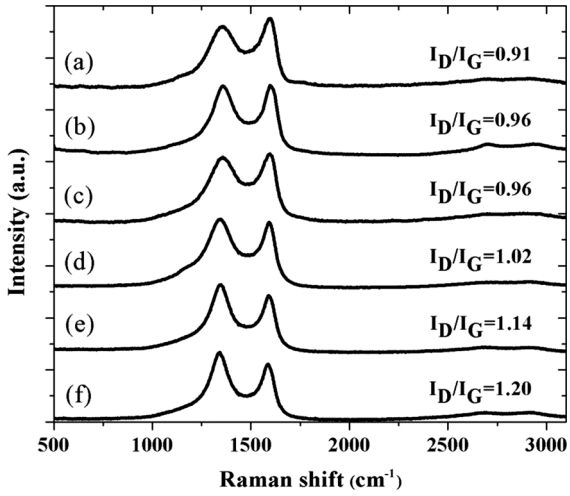

Fig. 3 Raman spectra of (*a*) as-deposited GO and annealed samples at (*b*) 200, (*c*) 400, (*d*) 600, (*e*) 800, and (*f*) 1000 °C, for 1 h

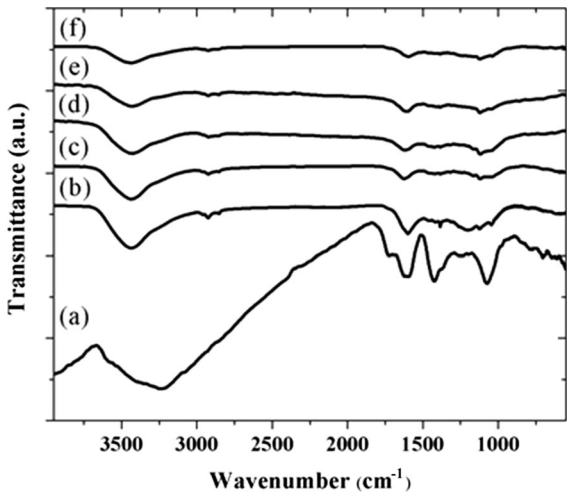

Fig. 4 FT-IR spectra of (*a*) the as-deposited GO and (*b–f*) samples annealed in the temperature range 200–1000 °C

stretching vibrations (1721 cm^{-1}), C=C stretching, skeletal vibrations of unoxidized graphitic domains (1620 cm^{-1}), O–H deformation (1421 cm^{-1}), C–OH stretching vibrations (1232 cm^{-1}), and C–O stretching vibrations (1072 cm^{-1}), all of which are usually observed in GO (Dong et al. 2013; Shen et al. 2011).

Figure 4b–f illustrates the evolution of the reduction process with the annealing temperature. It was seen that the absorption bands associated with the abovementioned oxygenated groups gradually decreased in intensity. Particularly, the stretching vibration band of the C=O group at 1721 cm^{-1} vanished entirely, even at the processing temperature of 200 °C.

As Raman spectroscopy, FT-IR was unable to detect IR bands of the oxidized copper, particularly those associated with the Cu–O bond vibrations of Cu_2O which is located at ~617 cm^{-1} (Necmi et al. 2005).

Morphology

After the heat treatment at 200–1000 °C, Cu_2O- or Cu–rGO nanocomposite was observed at the Cu foil surface, depending on the annealing temperature. In all cases, well-crystallized Cu_2O or Cu nanoparticles were obtained, as indicated by the XRD analyses.

Figures 5 and 6 reveal the annealing temperature strong effect on the morphology of Cu-based nanoparticles, as well as the GO network. In all cases, polydisperse nanoparticles were obtained, and they increased in size with annealing temperature; the particle mean size was 15, 25, 45, 90, and 600 nm for 200, 400, 600, 800, and 1000 °C, respectively.

Figure 5 displays FESEM images of representative samples prepared at 200 and 400 °C for 1 h. In this temperature range, the inorganic nanoparticles were predominantly cubic Cu_2O. The sample at 600 °C (omitted here) displays similar morphological features as those of 400 °C.

The FESEM images in Fig. 6 correspond to samples prepared at 800–1000 °C. In this temperature range, elemental Cu develops as the predominant inorganic phase nanoparticles.

As far as we know, there are no reports on Cu or Cu_2O nanoparticles synthesis by following a similar process as the one reported here, including reports on the graphene synthesis on Cu foil (Li et al. 2009; Wofford et al. 2015) or on Cu-evaporated thin films (Mattevi et al. 2011).

Recently, Glover et al. (Glover et al. 2011) reported the spontaneous formation of copper and silver nanoparticles at the surface of the corresponding metal object under ambient conditions. Therefore, it is quite probably that the studied nanoparticles here were developed from the preformed copper oxide nanoparticles, which grew during the GO-copper foil sample preparation. During the thermal process, the preformed nanoparticles diffused across the Cu foil surface on a thin layer of partly melted copper. Then

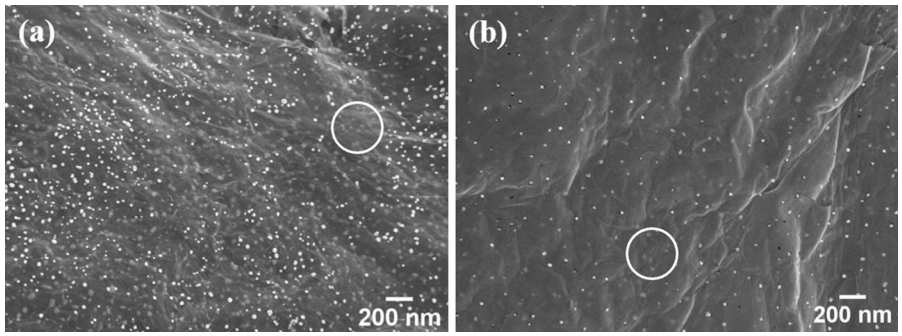

Fig. 5 FESEM images of samples annealed at (**a**) 200 and (**b**) 400 °C, for 1 h. It is seen that the nanocomposite comprises embedded (*circle*) and surfaced Cu_2O nanoparticles in rGO network

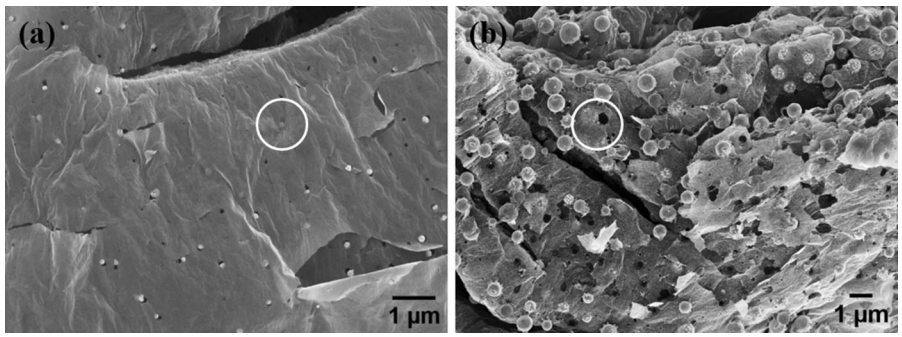

Fig. 6 FESEM images of samples annealed at (**a**) 800 and (**b**) 1000 °C for 1 h

they self-assemble to produce bigger nanostructures of copper oxide or elemental copper.

To explain the formation of Cu or Cu_2O as the predominant phase, we have assumed that copper oxide develops in the entire annealing temperature range, and that it transforms into Cu or Cu_2O through a carbothermal reduction process involving the gaseous species carbon monoxide (CO) and carbon dioxide (CO_2) (Goldstein and Mitchell 2011). In other words, it is very probable that copper oxide phases other than the native one, developed from the melted copper and oxygen interaction, oxygen (O_2) being produced during the GO thermal reduction (Chen and Yan 2010). Previous studies on the graphene oxide thermal reduction have demonstrated that O_2 and other gaseous species such as CO and CO_2 evolved during the thermal process, even at temperatures lower than 200 °C (Chuang et al. 2014; Ganguly et al. 2011).

According to the XRD and FESEM studies, the annealing temperature strongly affects the nanocomposite morphology and its phase composition. An additional effect can be noted by comparing FESEM images (Figs. 1a, 5 and 6). The initial sample (Fig. 1a) comprises crumpled GO sheets, which transform into smoothed and stacked rGO sheets after the thermal treatment (Figs. 5 and 6). Furthermore, the holed aspect of rGO sheets appears to suggest Cu nanoparticles consumed some amount of surrounding carbon to get a carbon coating. Notice that the hole size increases as annealing temperature does, following a similar trend as that of the Cu nanoparticle size.

The FESEM image (Fig. 6b) displays the striking morphology of the sample prepared at 1000 °C. It consists of Cu nanostructures decorating the rGO sheets and some holes on the rGO sheet. As in the previous samples treated at lower temperatures (Fig. 5), it is seen that the nanocomposite comprises embedded (circle) and surfaced Cu nanoparticles in rGO network.

Conclusions

We propose a novel and simple method to simultaneously reduce GO and decorate it with copper oxide or copper nanoparticles. The method consists of annealing, under an Ar atmosphere, the as-deposited GO sheets using a copper foil as the GO support. It was demonstrated that the Cu-based rGO sheets nanocomposite could be prepared at temperatures as low as 200 °C. Importantly, the Cu_2O and Cu can be obtained by varying the process temperature. In regard to the Cu nanoparticles stability, we suggested that they could be coated by rGO, but a further study should be addressed to corroborate this issue.

Acknowledgments This project is supported by the National Council of Science and Technology (CONACyT) No. CB2009-128723 and scholarship No. 355201. Also we are indebted with Institute of Science and Technology of Federal District (ICyT 326/11). The authors are very thankful to M. Sci. Adolfo Tavira Fuentes for the XRD measurements and also LANE-Cinvestav, especially Dr. Josué Romero Ibarra for the FESEM characterizations.

References

Allen MJ, Tung VC, Kaner RB (2009) Honeycomb carbon: a review of graphene. Chem Rev 110:132–145. doi:10.1021/cr900070d

Bai S, Shen X (2012) Graphene-inorganic nanocomposites. RSC Adv 2:64–98. doi:10.1039/C1RA00260K

Bose S, Kuila T, Mishra AK, Kim NH, Lee JH (2012) Dual role of glycine as a chemical functionalizer and a reducing agent in the preparation of graphene: an environmentally friendly method. J Mater Chem 22:9696–9703. doi:10.1039/C2JM00011C

Cai M, Thorpe D, Adamson DH, Schniepp HC (2012) Methods of graphite exfoliation. J Mater Chem 22:24992–25002. doi:10.1039/C2JM34517J

Casabianca LB, Shaibat MA, Cai WW, Park S, Piner R, Ruoff RS, Ishii Y (2010) NMR-based structural modeling of graphite oxide using multidimensional 13C solid-state NMR and ab initio chemical shift calculations. J Am Chem Soc 132:5672–5676. doi:10.1021/ja9030243

Chen W, Yan L (2010) Preparation of graphene by a low-temperature thermal reduction at atmosphere pressure. Nanoscale 2:559–563. doi:10.1039/B9NR00191C

Chen W, Yan L, Bangal PR (2010) Preparation of graphene by the rapid and mild thermal reduction of graphene oxide induced by microwaves. Carbon 48:1146–1152. doi:10.1016/j.carbon.2009.11.037

Choi BG, Huh YS, Park YC, Jung DH, Hong WH, Park H (2012) Enhanced transport properties in polymer electrolyte composite membranes with graphene oxide sheets. Carbon 50:5395–5402. doi:10.1016/j.carbon.2012.07.025

Chuang CH et al (2014) The effect of thermal reduction on the photoluminescence and electronic structures of graphene oxides. Sci Rep. doi:10.1038/srep04525

Compton OC, Nguyen ST (2010) Graphene oxide, highly reduced graphene oxide, and graphene: versatile building blocks for carbon-based materials. Small 6:711–723. doi:10.1002/smll.200901934

Deng S et al (2012) Reduced graphene oxide conjugated Cu2O nanowire mesocrystals for high-performance NO2 gas sensor. J Am Chem Soc 134:4905–4917. doi:10.1021/ja211683m

Dong J, Liu W, Li H, Su X, Tang X, Uher C (2013) In situ synthesis and thermoelectric properties of PbTe-graphene nanocomposites by utilizing a facile and novel wet chemical method. J Mater Chem A 1:12503–12511. doi:10.1039/C3TA12494K

Dong X et al (2014) Direct synthesis of RGO/Cu2O composite films on Cu foil for supercapacitors. J Alloy Compd 586:745–753. doi:10.1016/j.jallcom.2013.10.078

Dreyer DR, Park S, Bielawski CW, Ruoff RS (2010) The chemistry of graphene oxide. Chem Soc Rev 39:228–240. doi:10.1039/B917103G

Fernández-Merino MJ, Guardia L, Paredes JI, Villar-Rodil S, Solís-Fernández P, Martínez-Alonso A, Tascón JMD (2010) Vitamin C Is an ideal substitute for hydrazine in the reduction of graphene oxide suspensions. J Phys Chem C 114:6426–6432. doi:10.1021/jp100603h

Ganguly A, Sharma S, Papakonstantinou P, Hamilton J (2011) Probing the thermal deoxygenation of graphene oxide using high-resolution in situ X-ray-based spectroscopies. J Phys Chem C 115:17009–17019. doi:10.1021/jp203741y

Glover RD, Miller JM, Hutchison JE (2011) Generation of metal nanoparticles from silver and copper objects: nanoparticle dynamics on surfaces and potential sources of nanoparticles in the environment. ACS Nano 5:8950–8957. doi:10.1021/nn2031319

Goldstein EA, Mitchell RE (2011) Chemical kinetics of copper oxide reduction with carbon monoxide. Proc Combust Inst 33:2803–2810. doi:10.1016/j.proci.2010.06.080

Guo H-L, Wang X-F, Qian Q-Y, Wang F-B, Xia X-H (2009) A green approach to the synthesis of graphene nanosheets. ACS Nano 3:2653–2659. doi:10.1021/nn900227d

Hadadian M, Goharshadi E, Youssefi A (2014) Electrical conductivity, thermal conductivity, and rheological properties of graphene oxide-based nanofluids. J Nanopart Res 16:1–17. doi:10.1007/s11051-014-2788-1

Hien VX, Kim S-Y, Lee J-H, Kim J-J, Heo Y-W (2013) Growth of CuO nanowires on graphene-deposited Cu foil by thermal oxidation method. J Cryst Growth 384:100–106. doi:10.1016/j.jcrysgro.2013.09.019

Hu C, Zhai X, Liu L, Zhao Y, Jiang L, Qu L (2013) Spontaneous reduction and assembly of graphene oxide into three-dimensional graphene network on arbitrary conductive substrates. Sci Rep 3:2065. doi:10.1038/srep02065. http://www.nature.com/articles/srep02065#supplementary-information

Huh SH (2011) Thermal reduction of graphene oxide. In: Mikhailov S (ed) Physics and applications of graphene-experiments. InTech, New York

Hummers WS, Offeman RE (1958) Preparation of graphitic oxide. J Am Chem Soc 80:1339. doi:10.1021/ja01539a017

Li X et al (2009) Large-area synthesis of high-quality and uniform graphene films on copper foils. Science 324:1312–1314. doi:10.1126/science.1171245

Li M et al (2014) Graphene oxide/hydroxyapatite composite coatings fabricated by electrophoretic nanotechnology for biological applications. Carbon 67:185–197. doi:10.1016/j.carbon.2013.09.080

Liu H, Liu Y, Zhu D (2011) Chemical doping of graphene. J Mater Chem 21:3335–3345. doi:10.1039/C0JM02922J

Mai YJ, Wang XL, Xiang JY, Qiao YQ, Zhang D, Gu CD, Tu JP (2011) CuO/graphene composite as anode materials for lithium-ion batteries. Electrochim Acta 56:2306–2311. doi:10.1016/j.electacta.2010.11.036

Mattevi C, Kim H, Chhowalla M (2011) Physics and applications of graphene-experiments. J Mater Chem 21:3324–3334. doi:10.1039/C0JM02126A

Menchaca-Campos C et al (2013) Nylon/graphene oxide electrospun composite coating. Int J Polym Sci 2013:9. doi:10.1155/2013/621618

Moon IK, Lee J, Ruoff RS, Lee H (2010) Reduced graphene oxide by chemical graphitization. Nat Commun 1:73–78. http://www.nature.com/ncomms/journal/v1/n6/suppinfo/ncomms1067_S1.html

Na HG et al (2015) Reduced graphene oxide functionalized with Cu nanoparticles: fabrication, structure, and sensing properties. Thin Solid Films 588:11–18. doi:10.1016/j.tsf.2015.03.078

Necmi S, Tülay S, Şeyda H, Yasemin Ç (2005) Annealing effects on the properties of copper oxide thin films prepared by chemical deposition. Semicond Sci Technol 20:398

Neo CY, Ouyang J (2013) The production of organogels using graphene oxide as the gelator for use in high-performance quasi-solid state dye-sensitized solar cells. Carbon 54:48–57. doi:10.1016/j.carbon.2012.11.002

Notley SM (2012) Highly concentrated aqueous suspensions of graphene through ultrasonic exfoliation with continuous surfactant addition. Langmuir 28:14110–14113. doi:10.1021/la302750e

Park S, An J, Potts JR, Velamakanni A, Murali S, Ruoff RS (2011) Hydrazine-reduction of graphite- and graphene oxide. Carbon 49:3019–3023. doi:10.1016/j.carbon.2011.02.071

Pei S, Cheng H-M (2012) The reduction of graphene oxide. Carbon 50:3210–3228. doi:10.1016/j.carbon.2011.11.010

Shen J, Yan B, Shi M, Ma H, Li N, Ye M (2011) One step hydrothermal synthesis of TiO_2-reduced graphene oxide sheets. J Mater Chem 21:3415–3421. doi:10.1039/C0JM03542D

Shi W et al (2011) Achieving high specific charge capacitances in Fe3O4/reduced graphene oxide nanocomposites. J Mater Chem 21:3422–3427. doi:10.1039/C0JM03175E

Singh V, Joung D, Zhai L, Das S, Khondaker SI, Seal S (2011) Graphene based materials: past, present and future. Prog Mater Sci 56:1178–1271. doi:10.1016/j.pmatsci.2011.03.003

Sobon G et al (2012) Graphene oxide versus reduced graphene oxide as saturable absorbers for Er-doped passively mode-locked fiber laser. Opt Express 20:19463–19473. doi:10.1364/OE.20.019463

Some S, Kim Y, Yoon Y, Yoo H, Lee S, Park Y, Lee H (2013) High-Quality Reduced Graphene Oxide by a Dual-Function Chemical Reduction and Healing Process Sci Rep 3:1–15. doi:10.1038/srep01929. http://www.nature.com/srep/2013/130531/srep01929/abs/srep01929.html#supplementary-information

Stankovich S et al. (2006) Graphene-based composite materials. Nature 442:282–286. http://www.nature.com/nature/journal/v442/n7100/suppinfo/nature04969_S1.html

Stankovich S et al (2007) Synthesis of graphene-based nanosheets via chemical reduction of exfoliated graphite oxide. Carbon 45:1558–1565. doi:10.1016/j.carbon.2007.02.034

Wofford JM, Nie S, Thürmer K, McCarty KF, Dubon OD (2015) Influence of lattice orientation on growth and structure of graphene on Cu(0 0 1). Carbon 90:284–290 doi:10.1016/j.carbon.2015.03.056

Wu C-K, Wang G-J, Dai J-F (2013) Controlled functionalization of graphene oxide through surface modification with acetone. J Mater Sci 48:3436–3442. doi:10.1007/s10853-012-7131-6

Xu C, Wang X, Yang L, Wu Y (2009) Fabrication of a graphene–cuprous oxide composite. J Solid State Chem 182:2486–2490. doi:10.1016/j.jssc.2009.07.001

Xu C, Cui A, Xu Y, Fu X (2013) Graphene oxide–TiO_2 composite filtration membranes and their potential application for water purification. Carbon 62:465–471

Zhang Y, Ma H-L, Zhang Q, Peng J, Li J, Zhai M, Yu Z-Z (2012) Facile synthesis of well-dispersed graphene by [gamma]-ray induced reduction of graphene oxide. J Mater Chem 22:13064–13069. doi:10.1039/C2JM32231E

Zhao B et al (2012) Supercapacitor performances of thermally reduced graphene oxide. J Power Sour 198:423–427. doi:10.1016/j.jpowsour.2011.09.074

Zhenyuan J, Xiaoping S, Minzhi L, Hu Z, Guoxing Z, Kangmin C (2013) Synthesis of reduced graphene oxide/CeO_2 nanocomposites and their photocatalytic properties. Nanotechnology 24:115603